EAST EUROPEAN JOURNAL OF PHYSICS. **1.** 189-196 (2023)
DOI:10.26565/2312-4334-2023-1-25 ISSN 2312-4334

INFLUENCE OF DEPOSITION VOLTAGE ON STRONTIUM SULPHIDE DOPED SILVER FOR OPTOELECTRONIC APPLICATION†

Shaka O. Samuel[a,d], M. Lagbegha-ebi Frank[b], E.P. Ogherohwo[c], Arthur Ekpekpo[d], J.T. Zhimwang[e], Imosobomeh L. Ikhioya[f]*

[a]*Department of Science Laboratory Technology, Delta State University, Abraka, Delta State, Nigeria*
[b]*International Institute of Tourism and Hospitality, Yenagoa, Bayelsa State, Nigeria*
[c]*Federal University of Petroleum Resources, Effurun, Delta State, Nigeria*
[d]*Department of Physics, Delta State University, Abraka, Delta State, Nigeria*
[e]*Federal University of Lokoja, Nigeria*
[f]*Department of Physics and Astronomy, University of Nigeria, Nsukka, 410001, Enugu State, Nigeria*
**Corresponding Author e-mail: imosobomeh.ikhioya@unn.edu.ng*
Received December 19, 2022; revised January 17, 2023; accepted January 20, 2023

In the research electrochemical deposition technique was use in deposition of undoped SrS and doped SrS with silver were 0.01 mol of thioacetamide (C_2H_5NS), 0.1 mol of strontium chloride hexahydrate ($SrCl_2 \cdot 6H_2O$), and 0.01 mol of silver nitrate ($AgNO_3$) were utilized as the cationic, anionic, and dopant concentrations. The XRD spectra of the SrS and SrS doped silver showed prominent crystalline peaks at angles of 26.69°, 37.97°, 51.39°, and 65.56° for SrS and 26.42°, 33.42°, 37.98°, and 51.32° for SrS/Ag, respectively, with corresponding diffraction planes (111), (112), (200), and (211). However, the diffraction pattern shows that the peak intensity increases as the deposition voltage increases. The undoped SrS material morphology has a clove-like substance with precipitate; the large nano grain on the substrate's surface exhibits photon absorption but shows no traces of pinholes. When doped SrS is deposited at various precursor voltages, it forms uniform surfaces devoid of pinholes. The cell also penetrates the substrate being used for the deposition, as seen by the elemental makeup of the films. It was observed that SrS/Ag at 10V and 12V had little precipitate on the surfaces; this is because a carbon electrode was utilized, which tends to react with electrolyte at low voltages but does not do so at 14 V. The films show that when the deposition voltage increased, the electrical resistivity decreased from 1.42×10^9 to 1.37×10^9 Ω·m and the thickness decreased from 125.02 to 123.025 nm. This further led to an increase in conductivity from 7.04×10^8 to 7.29×10^8 S/m. It was discovered that the absorbance decreases as the electromagnetic radiation's wavelength grows and the deposition voltage rises. According to research done on the deposited material, its energy bandgap lies between 1.55 and 2.51 eV.
Keywords: *Undoped SrS; bandgap energy; XRD; SEM; EDX*
PACS: 42.55.Rz, 42.70.Qs, 87.64.Dz, 78.70.Dm, 83.85.Hf

1. INTRODUCTION

The current century has seen a fast increase in the need for non-stop, renewable energy sources and energy storage technologies [1]. Growing interest in solar cells and photovoltaic devices, which can replace and, if possible, outperform the inefficient systems of energy storage devices currently in vogue, is a result of the pressing demand for effective energy storage devices [2]. As a result, nano scientists and engineers have been working diligently over the years to create some trustworthy wide-bandgap metal chalcogenide that will lower the risk of exposure to harmful elements while also reducing the overall shortfall of energy consumption [3]. Transition metals have gained significant interest in the search for materials with strong potentials for electrochemical energy storage devices [4–7], as evidenced by the sharp rise in the number of studies on these metals in recent years [8]. Their stronger redox chemical valences for use in photovoltaic solar cells are one important factor that could have caused this. Due to their numerous existing applications, the SrS metal has been viewed as the most appealing over time. A substance with intriguing physical, chemical, and optoelectronic applications is strontium sulphide semiconductor. Materials made of strontium sulphide are used in anti-reflection coatings, temperature controllers in satellites, microelectronic devices, photoconductors, magnetic sensors, gas sensors, solar cells, interference filters, superconducting films, infrared (IR) detectors, polarizers, decorating, and anti-corrosive coatings [8–11].

In each of these applications, a semiconductor-based optoelectronic device is an essential part of the system. One of the key advantages of semiconductor devices is their compact design. A typical edge-emitting laser, for instance, measures roughly 500×250×100 m^3. A single wafer can be used to manufacture thousands of these devices. As a result, these coherent radiation sources are incredibly tiny even when packaged [15]. Gas lasers, for example, cannot be compared to semiconductor lasers in terms of size, modulation rates, application variety, or power consumption. Furthermore, semiconductor devices can be specifically tailored to meet the requirements of a given application by simply altering the composition of the several layers that make up the structure [16]. Out of all the purposes mentioned above, the usage of semiconductor devices in telecommunications has the biggest impact on how people live today. The extensive research and development that went into developing semiconductor devices for light emission and detection is what gave rise to these capabilities [17].

† ***Cite as:*** S.O. Samuel, Frank M. Lagbegha-ebi, E.P. Ogherohwo, A. Ekpekpo, J.T. Zhimwang, and I.L. Ikhioya, East Eur. J. Phys. **1**, 189 (2023), https://doi.org/10.26565/2312-4334-2023-1-25

Optical communications led to improvements in optoelectronics, such as the development of avalanche photodiodes, vertical-cavity surface-emitting lasers, semiconductor optical amplifiers, and optical modulators. Carrier-photon interactions are researched in the context of designing efficient and high-performance emitters and detectors. We suggested talking about how different metal dopants, the concentration of precursors, the temperature of precursors, and the voltage of the deposition with a time constant can change the semiconductor band structure to improve device attributes. Optoelectronic devices are widely used in a variety of applications nowadays and are widely available. Some of the parts of these devices include photo-detectors, optical amplifiers, and optical modulators, in addition to sources like light-emitting diodes (LEDs) and laser diodes. With the aid of these tools, photons may be produced, modulated, detected, and switched just like electrons in an electrical circuit [18].

Wide-gap semiconductors are necessary for modern optoelectronics because of their higher conductivity and transparency, according to Masaya et al. in (2021) [19]. The development of high-performance transparent electronic devices is significantly constrained by the major technological drawbacks of p-type transparent conducting materials, despite the fact that n-type TCMs have had tremendous success. In the current study, we hypothesize that the hybrid functional approach can produce transparent ambipolar conducting in SrS. A newly developed and incredibly effective electroluminescent phosphor material, Sey-Shing, (2019) SrS/Cu, was produced [20]. The EL characteristics of SrS/Cu can be varied by altering the co-dopant material. True blue is displayed by SrS/Cu devices that have been co-doped with Ag, but cyan is displayed by SrS/Cu thin film EL devices that have only been singly doped, with varying between 0.27 and 0.32 SrS/Cu, Ag has a significantly higher luminous efficiency than existing blue EL phosphors like (SrCa)Ga2S4/Ce and blue filtered SrS/Ce, ranging from 0.15 to 0.24 lm/W, when the hue is matched. It is projected that the color and brightness performance of the following generation of color TFEL displays will improve once SrS/Cu, Ag is put into production. The SrS/Ce phosphor was produced through solid-state diffusion, according to Vijay et al. in 2020 [21]. Powder X-ray diffraction, transmission electron microscopy, thermogravimetric analysis, and photoluminescence spectra were used to assess the product's properties. Photoluminescence spectra were also used to check the product's optical properties. Thermoluminescence and electron spin resonance investigations have also been conducted on the SrS/Ce phosphor. The broad TL glow curve exhibits three unique peaks, two of which are strong peaks at 137 and 275°C and one of which is a shoulder at 362°C. There are two defect centers visible at ambient temperature. One of them has an isotropic g-value of 2.0039, indicating that it belongs to a F+ center. There may be a connection between the F+ center and the 137°C TL peak.

Numerous research teams have reported their success in growing thin films using a range of techniques, including spray pyrolysis, solvothermal synthesis, ion beam assisted coating, chemical bath deposition, DC magnetron sputtering, spray pyrolysis, vacuum evaporation, thermal evaporation, SILAR, molecular beam epitaxy, and electrodeposition. In the current experiment, SrS and SrS/Ag material was deposited at room temperature using the electrodeposition approach since it offers comparative advantages over other methods in terms of economy, convenience, and ability to deposit vast regions of films [15-21]. It is extensively used to deposit different metal chalcogenides and is regularly employed with electrically conductive materials such conductive polymers, alloys, and metals. On the surface of the substrate, homogeneous deposits are produced by managing the rate at which precipitates emerge from the solution. Simple growth control in terms of thickness, rate of deposition, and film quality is additionally made possible by modifying the pH, temperature, deposition voltage and concentration of the solution bath. Dopants attempt to change the electrical, optical, and electronic properties of semiconducting materials [12-14].

Silver was used as a dopant to increase the conductivity of the material by reducing the energy needed for electrons to go from the valence band to the conduction band. The investigation's findings present materials that are suitable for usage in optoelectronic and solar cell applications.

2. EXPERIMENTAL DETAIL

Chemicals that have been evaluated analytically are purchased and used without further purification. FTO conductive glass served as the substrate. The substrates underwent acetone and methanol immersion, distilled water washing, and a 30-minute treatment with an ultrasonic bath in acetone. After being cleansed in distilled water, they were baked to dry. Thioacetamide (C_2H_5NS), 0.1 mol of strontium chloride hexahydrate (SrCl2.6H2O), and 0.01 mol of silver nitrate (AgNO3) were utilized as the cationic, anionic, and dopant concentrations. The films were deposited using the electrochemical deposition process. The electrochemical apparatus had a bath that included distilled water, 20 ml of each cationic and anionic precursor, and a 100 ml beaker. The cathode and anode materials were fluorine-doped tin oxide and carbon, and direct current voltage was generated by the power supply. The chamber has three electrode configurations: a working electrode, an electrode made of silver-silver chloride (Ag/AgCl), which serves as the reference electrode, and platinum mesh as the positive electrode. For all depositions, the fluorine-doped tin oxide substrate was positioned perpendicular to the chamber, including the counter and reference electrodes. For 10 seconds, the synthesis was conducted at a potentiostat setting of 200 mV against SCE. As a result, the synthesized films were cleaned and dried. The target materials, which consist of equal amounts (20 ml) of strontium chloride, thioacetamide, and 10 ml of silver nitrate solutions, were metered into the beakers during the deposition process. After the syntheses, the films were heated and annealed for 30 minutes to remove concentrated tensions under a variable voltage supply of 10V to 14V. By adding 10 ml of 0.01 mol of silver nitrate to the electrochemical bath, the silver nitrate dopant was introduced. The samples were collected at pH levels of 7.0 and room temperature. Scanning electron microscopy, DW-XRD 2700A X-ray diffractometer

with Cu-Kα line (λ = 1.54184 Å) in 2θ range from 10° - 80°, a four-point probe (Model T345), and a UV-1800 visible spectrophotometer was used to characterize the prepared SrS and SrS/Ag films for their surface morphological, structural, elemental, electrical, and optical properties.

3. RESULTS AND DISCUSSION

3.1. XRD study of SrS and SrS doped silver at various deposition voltages for optoelectronic application

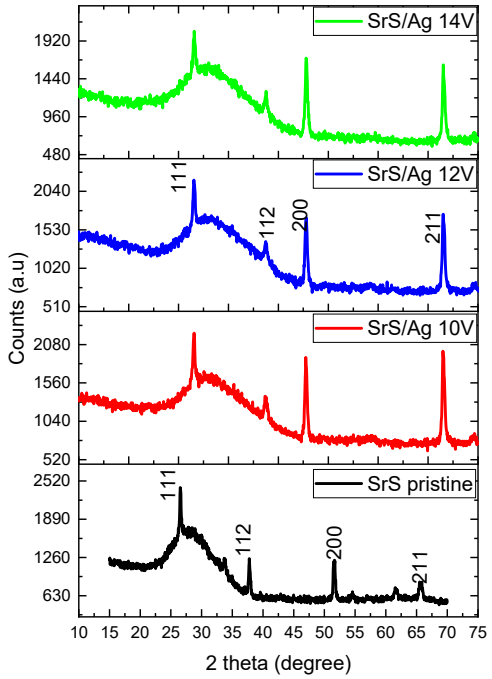

Figure 1. XRD spectrum

The XRD spectra of the SrS and SrS doped silver thin films in Figure 1 showed prominent crystalline peaks at angles of 26.69°, 37.97°, 51.39°, and 65.56° for SrS and 26.42°, 33.42°, 37.98°, and 51.32° for SrS/Ag, respectively, with corresponding diffraction planes (111), (112), (200), and (211).

However, the diffraction pattern shows that the peak intensity increases as the deposition voltage increases. Cell shrinkage may result from interstitial cation or solvent molecule removal, a rise in the precursor molecules' deposition voltage, or both. The crystallite of SrS and SrS doped silver thin films was identified using Debye Scherrer's formula;

$$D = \frac{K\lambda}{\beta cos(\theta)} \quad (1)$$

Where θ is Bragg's angle, β is FWHM, λ is the X-ray wavelength, K = 0.94, and D is the crystallite size.

Important factors like crystallite size and d-spacing are summarized in Table 1. As the deposition voltage rises, the size of SrS and SrS-doped silver crystallites also rises. Due to the restriction of crystallite motion at the interface between the dopant and host crystallite brought on by stress generation, the doped SrS has a smaller value of crystallite size than the undoped SrS.

Table 1. Structural parameters of SrS and SrS/Ag

Sample	2θ (degree)	d (spacing) Å	Lattice constant ()	(β) FWHM	(hkl)	Grain Size(D) nm	Dislocation density, σ lines/m^2
SrS pristine	26.6971	3.3360	5.7781	0.1851	111	7.6958	5.1445
	37.9741	2.3672	4.7345	0.1851	112	7.9188	4.9700
	51.3944	1.7762	3.5524	0.1851	200	8.3100	4.8648
	65.5611	1.4225	3.1809	0.1851	211	8.9066	4.3940
SrS/Ag 10V	26.4226	3.3700	5.8371	0.3840	111	3.7089	2.2143
	33.5574	2.6680	5.3361	0.3840	112	3.7713	2.1417
	37.9823	2.3667	4.7335	0.3840	200	3.8186	2.0890
	51.3258	1.7784	3.9767	0.3840	211	4.0060	1.8982
SrS/Ag 12V	26.4226	3.3700	5.8371	0.4136	111	3.4433	2.2148
	33.5574	2.6680	5.3361	0.4136	112	3.5013	2.1421
	37.9823	2.3667	4.7335	0.4136	200	3.5452	2.0894
	51.3258	1.7784	3.9767	0.4136	211	3.7191	1.8986
SrS/Ag 14V	26.4226	3.3700	5.8371	0.3616	111	3.9384	1.9639
	33.5574	2.6680	5.3361	0.3616	112	4.0046	1.8994
	37.9823	2.3667	4.7335	0.3616	200	4.0549	1.8527
	51.3258	1.7784	3.9767	0.3616	211	4.2538	1.6835

3.2. Surface morphology of SrS and SrS doped silver at various deposition voltages for optoelectronic application

The surface morphology of undoped and doped SrS materials is shown in Figure 2. The undoped SrS material morphology can be seen in the micrograph as clove-like substance with precipitate; the large nano grain on the substrate's surface exhibits photon absorption but shows no traces of pinholes.

When doped SrS is deposited at various precursor voltages, it forms uniform surfaces devoid of pinholes. The cell also penetrates the substrate being used for the deposition, as seen by the elemental makeup of the films. It was observed that SrS/Ag at 10V and 12V had little precipitate on the surfaces; this is because a carbon electrode was utilized, which tends to react with electrolyte at low voltages but does not do so at 14 V. In contrast to other nanoparticles, the SrS/Ag at 14 V is devoid of precipitation, and the nanoparticle is clearer. The material that was deposited will make a good candidate for photovoltaic and other applications due to its surface shape. The elemental composition of SrS that has not been doped

and SrS that has been doped with silver is shown in Figure 3 and Table 2. The spectrum clearly demonstrates that Sr, S, and Ag were present on the substrate, and the presence of other elements on the spectrum is due to the use of the FTO substrate, which contains additional elements, as the substrate for the deposition.

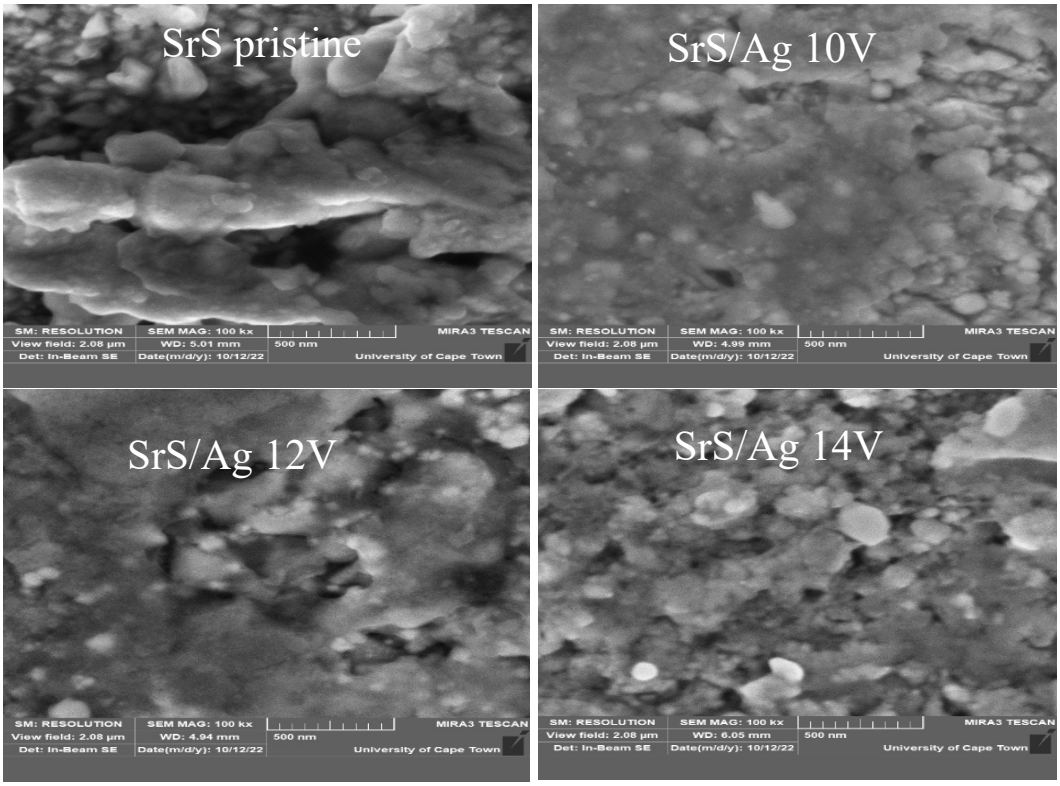

Figure 2. SEM micrograph of SRS/Ag

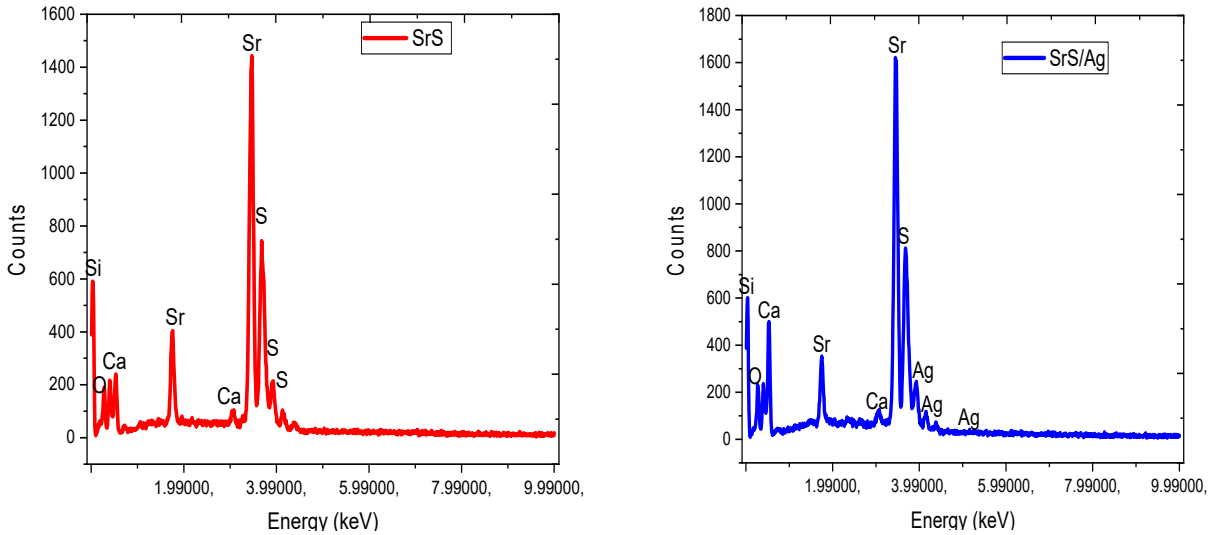

Figure 3. SrS and SrS/Ag EDX plots

Table 2. EDX spectra atomic weight percentages of the constituent elements.

Strontium Sulphide		**Strontium Sulphide doped Silver**	
Component	**Atomic Weight (%)**	**Component**	**Atomic Weight (%)**
Strontium	54.07	Strontium	58.30
Sulphide	24.01	Sulphide	19.08
Silicon	12.01	Silicon	10.0
Calcium	6.99	Calcium	3.60
Oxygen	3.01	Oxygen	2.00
-	-	Silver	7.02

3.3. Electrical study of SrS and SrS/Ag for optoelectronic application

The electrical analysis of silver-doped and undoped SrS is shown in Figure 3 and Table 3. The films show that when the deposition voltage increased, the electrical resistivity decreased from 1.42×10^9 to 1.37×10^9 Ω·m and the thickness decreased from 125.02 to 123.025 nm. This further led to an increase in conductivity from 7.04×10^8 to 7.29×10^8 S/m. Low resistance and high conductivity of the material will be useful for optoelectronic applications. As sheet thickness is reduced, resistivity declines and conductivity increase, as seen in Figure 4 (a). Synthesized films are a preferable option for photovoltaic and solar cell applications. Plots of resistivity and conductivity versus deposition voltage are shown. Figure 4 (b) shows that resistivity increases while conductivity decreases.

Table 3. Electrical properties of SrS and SrS doped silver at various deposition voltages for optoelectronic application

Films	Thickness, t (nm)	Resistivity, (Ω·m)	Conductivity, (S/m)
SrS	125.02	1.32×10^9	7.57×10^8
SrS/Ag 10V	124.10	1.42×10^9	7.04×10^8
SrS/Ag 12V	123.11	1.39×10^9	7.19×10^8
SrS/Ag 14V	123.05	1.37×10^9	7.29×10^8

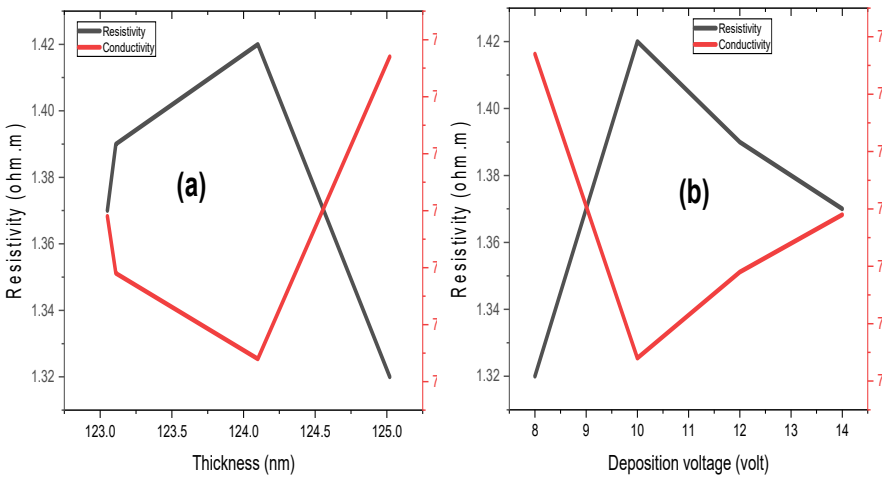

Figure 4. (a) resistivity and conductivity Vs thickness (b) resistivity and conductivity Vs deposition voltage

3.4. Optical study of SrS and SrS/Ag material deposited at the different voltages for optoelectronic application

Plots of the absorbance, transmittance, and reflectance of silver-doped SrS and undoped SrS are shown in Figure 5 for various deposition voltages between 10 and 14 volts. It is extremely obvious from Figure 5(a) that as light passes through the film and into the cells, the light is absorbed, making the material suitable for optoelectronic application. The SrS that was not doped had the maximum absorbance because it absorbed lighter than others. It was discovered that the absorbance decreases as the electromagnetic radiation's wavelength grows and the deposition voltage rises. Figure 5(b) shows that the undoped SrS has the lowest transmittance in the spectra while the doped SrS with silver deposited at 14 V has the highest transmittance in the spectra as the transmittance increases with increase in the deposition voltage and a corresponding increase in the wavelength of electromagnetic radiation. The reflectance of the material placed at various voltages is shown in Figure 5(c). Deposition voltage has a significant impact on SrS films because it causes a drop in the reflectance of SrS that has been doped with silver. A better material for optoelectronic applications is that which was deposited using 12V since it has the maximum reflectance.

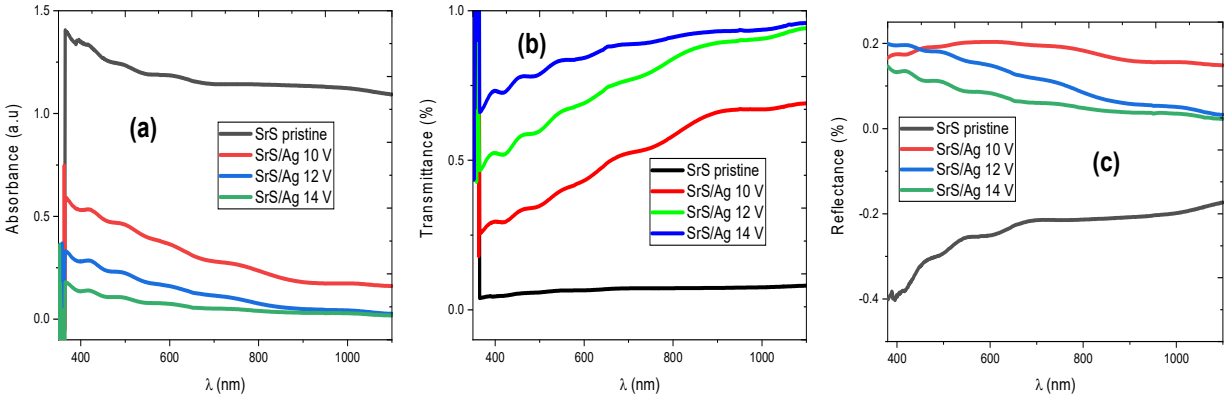

Figure 5. (a) absorbance, (b) transmittance, and (c) reflectance Vs wavelength

The plot of (hv)2 as a function of hv as shown in Figure 6 was used to determine the energy bandgap for undoped SrS and doped SrS deposited at various deposition voltages. According to research done on the deposited material, its energy bandgap lies between 1.55 and 2.51 eV. Due to the influence of the silver dopant on SrS, which was simulated as a substitutional dopant in its lattice location, it was determined that the bandgap energy for doped decreased from 2.10 to 2.51 eV. This doped material will be a promising material for optoelectronic and other applications because of the energy bandgap it displays.

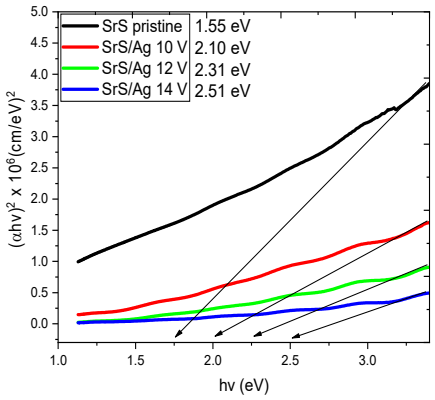

Figure 6. absorption coefficient square Vs photon energy

Plots of refractive index for undoped and doped SrS deposited at various deposition voltages are shown in Figure 7 (a). There was a rise in the refractive index of both doped and undoped material, as seen in the refractive index Vs hv spectra. It was observed from the spectra that an increase in the deposition voltage caused a reduction in the material's refractive index, and a decrease in the deposition voltage determined the usual scattering behavior of the films. For all of the produced films in Figure 7 (b), the coefficient of extinction increases as the photon energy increases. When compared to the films created at 12V and 14V, the undoped and doped SrS deposited with 10V certified high coefficient of extinction values. This rise in coefficient absorption can be coupled with a decline in transmission and an increase in the extinction value for the material with lower deposition voltage. The graph of the optical conductivity of doped and undoped SrS is shown in Figure 7 (c). Due to the high absorbance value of the synthesized material, which will eventually function as a superior material for optoelectronic applications, all the films recorded a moderate optical conductivity.

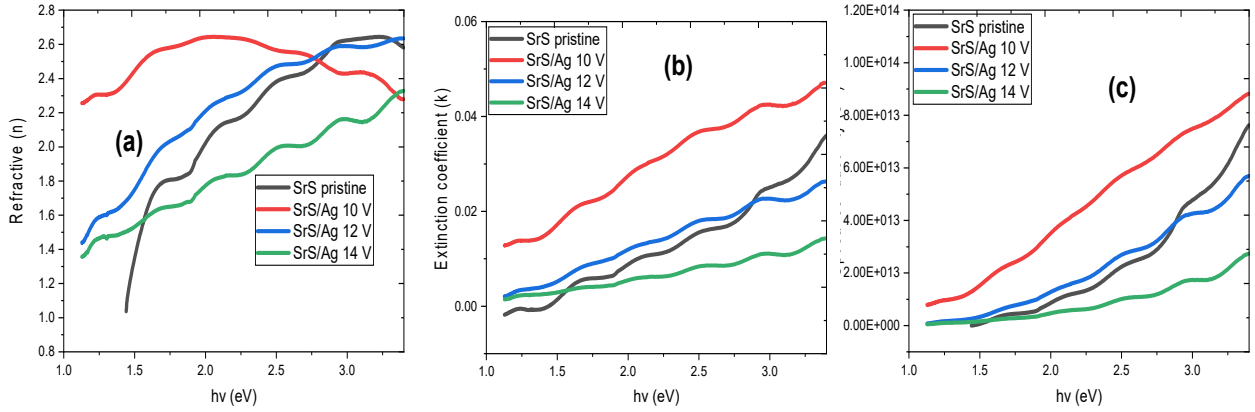

Figure 7. (a) refractive index, (b) extinction coefficient, (c) optical conductivity Vs photon energy

The doped and undoped SrS deposited at various deposition voltages are shown in Figure 8.

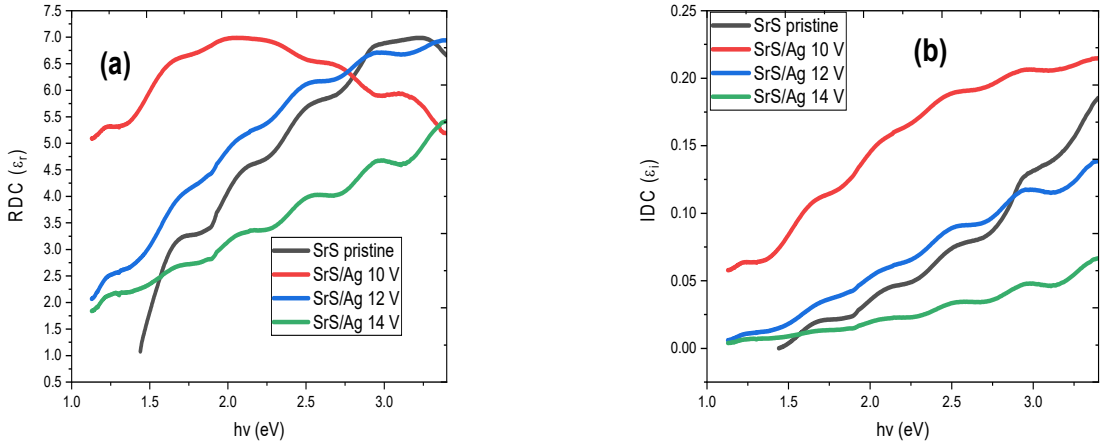

Figure 8. (a) real and (b) imaginary dielectric constant Vs photon energy

The dielectric loss demonstrates the loss of electrical energy in the form of thermal energy, whereas the dielectric constant shows how well dielectric materials store electrical energy (see Figure 8). Permittivity develops into a complex variable with real and made-up components in many modern fields. The real part (r) determines the level of polarization,

whereas the imaginary part (i) is related to dielectric losses. R's value rises as polarization does. The frequency has an effect on the dielectric constant. As frequency rises, the value declines because polarization mechanisms can no longer keep up with the fast-changing field. The amount of energy that has been used or consumed is represented by the imaginary component, which is always positive. As photon radiation increased, the actual portion of the material deposited rose dramatically, as shown in the spectra. The material is a strong candidate for optoelectronic applications since the real and imaginary properties of dielectric materials were improved by a deposition voltage.

4. CONCLUSIONS

We have successfully deposited undoped SrS and doped SrS with silver via electrochemical deposition technique. The XRD spectra of the SrS and SrS doped silver showed prominent crystalline peaks at angles of 26.69°, 37.97°, 51.39°, and 65.56° for SrS and 26.42°, 33.42°, 37.98°, and 51.32° for SrS/Ag, respectively, with corresponding diffraction planes (111), (112), (200), and (211). However, the diffraction pattern shows that the peak intensity increases as the deposition voltage increases. As the deposition voltage rises, the size of SrS and SrS-doped silver crystallites also rises. Due to the restriction of crystallite motion at the interface between the dopant and host crystallite brought on by stress generation, the doped SrS has a smaller value of crystallite size than the undoped SrS. The undoped SrS material morphology can be seen in the micrograph as clove-like substance with precipitate; the large nano grain on the substrate's surface exhibits photon absorption but shows no traces of pinholes. When doped SrS is deposited at various precursor voltages, it forms uniform surfaces devoid of pinholes. The cell also penetrates the substrate being used for the deposition, as seen by the elemental makeup of the films. It was observed that SrS/Ag at 10V and 12 V had little precipitate on the surfaces; this is because a carbon electrode was utilized, which tends to react with electrolyte at low voltages but does not do so at 14 V. The films show that when the deposition voltage increased, the electrical resistivity decreased from 1.42×10^{9} to 1.37×10^{9} Ω·m and the thickness decreased from 125.02 to 123.025 nm. This further led to an increase in conductivity from 7.04×10^{8} to 7.29×10^{8} S/m. It was discovered that the absorbance decreases as the electromagnetic radiation's wavelength grows and the deposition voltage rises. The undoped SrS has the lowest transmittance in the spectra while the doped SrS with silver deposited at 14V has the highest transmittance in the spectra as the transmittance increases with increase in the deposition voltage and a corresponding increase in the wavelength of electromagnetic radiation. According to research done on the deposited material, its energy bandgap lies between 1.55 and 2.51 eV. Due to the influence of the silver dopant on SrS, which was simulated as a substitutional dopant in its lattice location, it was determined that the bandgap energy for doped decreased from 2.10 to 2.51 eV.

ORCID IDs

Imosobomeh L. Ikhioya, https://orcid.org/0000-0002-5959-4427

REFERENCE

[1] A. Chaves, J.G. Azadani, H. Alsalman, D.R. da Costa, R. Frisenda, A.J. Chaves, S.H. Song, et al., "Bandgap engineering of two-dimensional semiconductor materials", npj 2D Mater. Appl. **4**, 29 (2020). https://doi.org/10.1038/s41699-020-00162-4

[2] M. Seifrid, G.N.M. Reddy, B.F. Chmelka, and G.C. Bazan, "Insight into the structures and dynamics of organic semiconductors through solid-state NMR spectroscopy", Nat. Rev. Mater. **5**, 910–930 (2020). https://doi.org/10.1038/s41578-020-00232-5

[3] J. Shi, J. Zhang, L. Yang, M. Qu, D.-C. Qi, and K.H.L. Zhang, "Wide Bandgap Oxide Semiconductors: from Materials Physics to Optoelectronic Devices", Advanced materials, **33**, 2006230 (2021). https://doi.org/10.1002/adma.202006230

[4] P.E. Agbo, and P.A. Nwofe, "Comprehensive studies on the optical properties of ZnO-core shell thin films", J. Nanotechnol. Adv. Mater, **3**(2), 63–97 (2015). https://www.naturalspublishing.com/files/published/7l62lvt2v9965a.pdf

[5] S. Gedi, V.R.M. Reddy, C. Park, J. Chan-Wook, and R.K.T. Reddy, "Comprehensive optical studies on SnS layers synthesized by chemical bath deposition", Optical Materials, **42**, 468–475 (2015). https://doi.org/10.1016/j.optmat.2015.01.043

[6] M.H. Suhail, and R.A. Ahmed, "Structural, optical and electrical properties of doped copper ZnS thin films prepared by chemical spray pyrolysis technique", Advances in Applied Science Research, **5**(5), 139-147 (2014). https://www.primescholars.com/articles/avo-analysis-of-3d-seismic-data-at-gfield-norway.pdf

[7] W.D. Callister, and D.G. Rethwisch, *Materials science and engineering*, vol. 5, (John Wiley & Sons, NY, 2011).

[8] D. Zhao, S. Sathasivam, J. Li, and C.J. Carmalt, "Transparent and Conductive Molybdenum-Doped ZnO Thin Films via Chemical Vapor Deposition", ACS Applied Electronic Materials, **2**(1), 120-125 (2020). https://doi.org/10.1021/acsaelm.9b00647

[9] I.L. Ikhioya, and A.J. Ekpunobi, "Electrical and Structural Properties of ZnSe Thin Films by Electrodeposition Technique", Journal of the Nigerian Association of Mathematical Physics, **29**, 325-330 (2015). https://www.researchgate.net/profile/Imosobomeh-Ikhioya/publication/323316123_of_NAMP_Electrical_and_Structural_Properties_of_ZnSe_Thin_Films_by_Electrodeposition_Technique/links/5a8d63c10f7e9b27c5b4adbc/of-NAMP-Electrical-and-Structural-Properties-of-ZnSe-Thin-Films-by-Electrodeposition-Technique.pdf

[10] I.I. Lucky, D.N. Okoli, and A.J. Ekpunobi, "Effect Of Temperature On SnZnSe Semiconductor Thin Films For Photovoltaic Application", SSRG International Journal of Applied Physics, **6**(2), 55-67 (2019). https://doi.org/10.14445/23500301/IJAP-V6I2P109

[11] I.I. Lucky, E.M. Chigozirim, O.D.O, and A.C. Rita, "The Influence of Precursor Temperature on The Properties of Erbium-Doped Zirconium Telluride Thin Film Material Via Electrochemical Deposition", SSRG International Journal of Applied Physics, **7**(1), 102-109 (2020). https://doi.org/10.14445/23500301/IJAP-V7I1P115

[12] I.L. Ikhioya, A.C. Nkele, E.M. Chigozirim, S.O. Aisida, M. Maaza, and F.I. Ezema, "Effects of Erbium on the Properties of Electrochemically-Deposited Zirconium Telluride Thin Films," Nanoarchitectonics, **2**(1), 18-26 (2021). https://doi.org/10.37256/nat.212021503

[13] I.L. Ikhioya, A.C. Nkele, C.F. Okoro, C. Obasi, G.M. Whyte, M. Maaza, and F.I. Ezema, "Effect of temperature on the morphological, structural and optical properties of electrodeposited Yb-doped $ZrSe_2$ thin films", Optik, **220**, 165180 (2020). https://doi.org/10.1016/j.ijleo.2020.165180

[14] I.L. Ikhioya, A.C. Nkele, S.N. Ezema, M. Maaza, and F. Ezema, "A study on the effects of varying concentrations on the properties of ytterbium-doped cobalt selenide thin films", Optical Materials, **101**, 109731 (2020). https://doi.org/10.1016/j.optmat.2020.109731

[15] X.-Z. Li, Y.-Y. Gu, H.-Q. Cheng, and X.-M. Meng, "Van der Waals Epitaxial Two-dimensional $CdS_xSe_{(1-x)}$ Semiconductor Alloys with Tunable-composition and Application to Flexible Optoelectronics", Nanoscale, **9**(36), 13786–13793 (2017). https://doi.org/10.1039/c7nr04968d

[16] S.H. Lee, S.B. Kim, Y.-J. Moon, S.M. Kim, H.J. Jung, M.S. Seo, K.M. Lee et al., "High-responsivity Deep Ultraviolet-selective Photodetectors Using Ultrathin Gallium Oxide Films", ACS Photonics, **4**(11), 2937-2943 (2017). https://doi.org/10.1021/acsphotonics.7b01054

[17] J. Yang, W. Yu, Z. Pan, Q. Yu, Q. Yin, L. Guo, Y. Zhao, et al, "Ultra-broadband Flexible Photodetector Based on Topological Crystalline Insulator SnTe with High Responsivity", Small, **14**(37), 1802598 (2018). https://doi.org/10.1002/smll.201802598

[18] V.E. Zaikova, N.V. Melnikova, A.V. Tebenkov, A.A. Mirzorakhimov, O.P. Shchetnikov, A.N. Babushkin, and G.V. Sukhanova, "Electrical Properties of Polycrystalline Materials from the System Cu-As-Ge-Se under High Pressure Condition", Journal of Physics: Conf. Series, **917**, 082009 (2017). https://doi.org/10.1088/1742-6596/917/8/082009

[19] M. Hamada, K. Matsuura, T. Hamada, I. Muneta, K. Kakushima, K. Tsutsui, and H. Wakabayashi, "ZrS_2 Symmetrical-ambipolar FETs with Near-midgap TiN Film for both Top-gate Electrode and Schottky-barrier Contact", Jpn. J. Appl. Phys. **60**, SBBH05 (2021). https://doi.org/10.35848/1347-4065/abd6d7

[20] S. Sey-Shing, "A New Blue Emitting TFEL Phosphor: SrS: Cu", Displays, **19**(4), 145-149 (2019). https://doi.org/10.1016/S0141-9382(98)00044-4

[21] S. Vijay, T. K. Gundu, J. M. Rao, and Z. Jun-Jie, "Synthesis and characterization of Ce-Doped SrS Phosphors", Radiation Effects and Defects in Solids, **160**(7), 265-274 (2005). https://doi.org/10.1080/10420150500375534

ВПЛИВ НАПРУГИ ОСАДЖЕННЯ НА ЛЕГОВАНИЙ СРІБЛОМ СУЛЬФІД СТРОНЦІЮ ДЛЯ ОПТОЕЛЕКТРОННОГО ЗАСТОСУВАННЯ

Шака О. Самуель[a,d], М. Лагбегха-ебі Франк[b], Е.П. Огерохво[c], Артур Екпекпо[d], Дж.Т. Джимванг[e], Імособоме Л. Іхіоя[f]

[a]*Відділ наукових лабораторних технологій, Університет штату Дельта, Абрака, штат Дельта, Нігерія*

[b]*Міжнародний інститут туризму та гостинності, Йенагоа, штат Байелса, Нігерія*

[c]*Федеральний університет нафтових ресурсів, Еффурун, штат Дельта, Нігерія*

[d]*Кафедра фізики, Університет штату Дельта, Абрака, штат Дельта, Нігерія*

[e]*Федеральний університет Локоджі, Нігерія*

[f]*Департамент фізики та астрономії, Університет Нігерії, Нсукка, 410001, штат Енугу, Нігерія*

У дослідницькій методиці електрохімічного осадження використовували нелегований SrS і легований SrS сріблом: 0,01 моль тіоацетаміду (C_2H_5NS), 0,1 моль гексагідрату хлориду стронцію ($SrCl_2{,}6H_2O$) і 0,01 моль нітрату срібла ($AgNO_3$) концентрації катіонів, аніонів і допантів. Рентгенівські спектри срібла, легованого SrS та SrS, показали помітні кристалічні піки під кутами 26,69°, 37,97°, 51,39° та 65,56° для SrS та 26,42°, 33,42°, 37,98° та 51,32° для SrS/Ag відповідно , з відповідними площинами дифракції (111), (112), (200) і (211). Однак дифракційна картина показує, що пікова інтенсивність зростає зі збільшенням напруги осадження. Морфологія нелегованого матеріалу SrS має гвоздикоподібну речовину з осадом; велике нанозерно на поверхні підкладки демонструє поглинання фотонів, але не має слідів точкових отворів. Коли легований SrS осаджується при різних початкових напругах, він утворює однорідні поверхні без точкових отворів. Клітина також проникає в субстрат, який використовується для осадження, як видно з елементного складу плівок. Було помічено, що SrS/Ag при 10 В і 12 В мало осаду на поверхнях; це пояснюється тим, що використовувався вугільний електрод, який має тенденцію реагувати з електролітом при низькій напрузі, але не реагує при 14 В. Плівки показують, що коли напруга осадження зросла, питомий електричний опір зменшився з $1{,}42\times10^9$ до $1{,}37\times10^9$ Ом·м, а товщина зменшилася з 125,02 до 123,025 нм. Це додатково призвело до збільшення провідності з 7,04×108 до 7,29×108 См/м. Було виявлено, що поглинання зменшується зі збільшенням довжини хвилі електромагнітного випромінювання та підвищенням напруги осадження. Згідно з дослідженнями, проведеними на осадженому матеріалі, його ширина забороненої зони становить від 1,55 до 2,51 еВ.

Ключові слова: *нелегований SrS; заборонена зона; XRD; SEM; EDX*